Cell Reports, Volume *42*

Supplemental information

Organelle interactions compartmentalize hepatic fatty acid trafficking and metabolism

Charles P. Najt, Santosh Adhikari, Timothy D. Heden, Wenqi Cui, Erica R. Gansemer, Adam J. Rauckhorst, Todd W. Markowski, LeeAnn Higgins, Evan W. Kerr, Matthew D. Boyum, Jonas Alvarez, Sophia Brunko, Dushyant Mehra, Elias M. Puchner, Eric B. Taylor, and Douglas G. Mashek

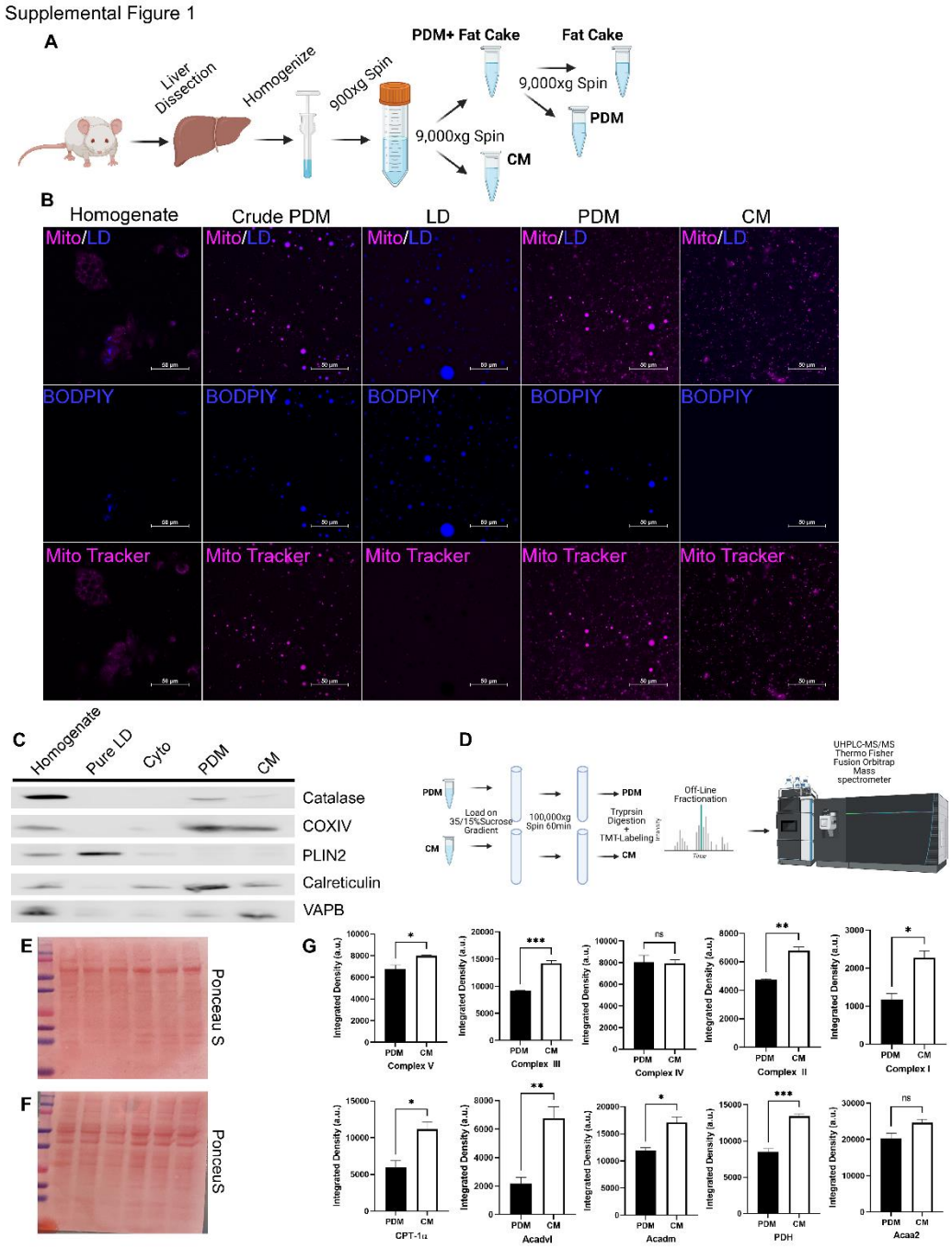

Figure S1. Isolation of CM and PDM from mouse liver (Related to Figure 1-2 and 4).

(A) Schematic of PDM and CM isolation from mouse hepatic tissue. Liver was dissected from mice and homogenized with glass-Teflon Dounce homogenizer. Low-speed centrifugation separated the fat layer containing PDM from supernatant containing CM. High-speed centrifugation stripped PDM from LDs and pelleted CM from the supernatant.

(B) Confocal images of crude and isolated organelle fractions. LDs were marked by the neutral LD stain Autodot and mitochondria by MitoTracker deep red dye.

(C) Immunoblotting of cellular fractions to determine the purity of CM and PDM. Fractions were probed for catalase (peroxisome), COXIV (mitochondria), PLIN2 (LD), calreticulin (ER/MAM), and VAP-B (MAM).
(D) Schematic showing the further purification steps taken prior to LC-MS/MS, protein digestion, isobaric labeling of peptides, offline fractionation, and LC-MS/MS.
(E) Ponceu S staining of total protein to normalize blots in Figure 1I.
(F) Ponceu S staining of total protein to normalize blots in Figure 2G.
(G) Quantification of Immunoblotting in Figure 1I normalized to total protein loading in E.

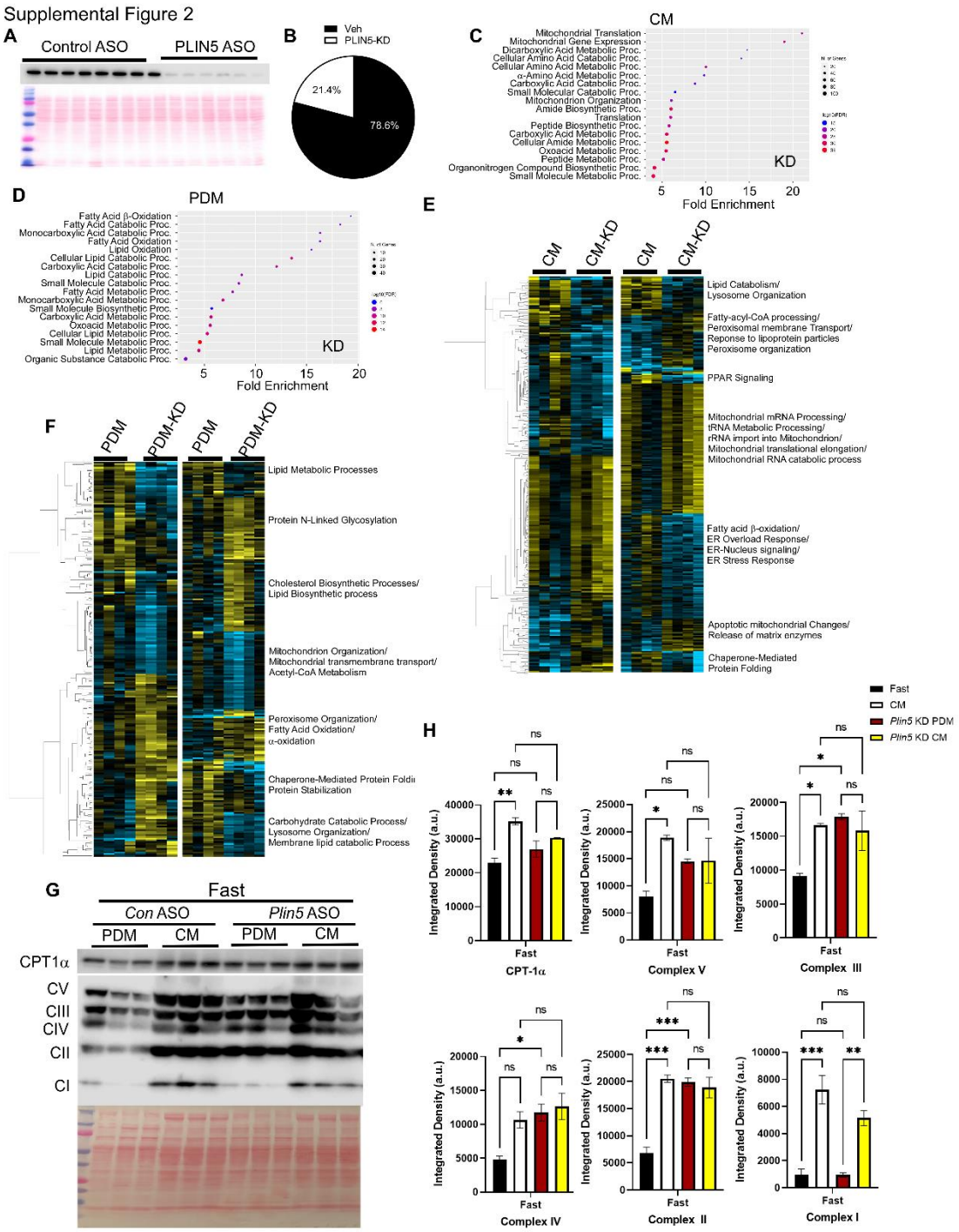

Figure S2. PLIN5 knockdown impacts cytosolic and peridroplet proteomes (Related to Figure 3).

(A) Immunoblotting of control and PLIN5 ASO-treated hepatic tissue samples to confirm PLIN5 knockdown.

(B) Quantitative proteomics was performed on CM and PDM fractions isolated from control and PLIN5 ASO treated and overnight fasted mice. The effect of PLIN5 knockdown on CM and PDM proteomes as part of the entire data set is depicted in a pie chart. n=4.

(C) GO term pathway analysis of all significant proteins detected in the CM fraction (Control CM vs PLIN5 KD).
(D) GO term pathway analysis of all significant proteins detected in the PDM fraction (Control PDM vs PLIN5 knockdown PDM).
(E) Hierarchical clustering of proteins significantly different between CM and PLIN5 knockdown CM across replicate fractions [threshold for clustered proteins was determined by significance between groups]. Proteins were further grouped using k-means statistics breaking the CM and PLIN5 knockdown CM significant genes into 10 protein clusters. The clustered proteins were mapped to specific metabolic pathways using Panther Classification Overrepresentation testing.
(F) Left: Hierarchical clustering of proteins significantly different between PDM and PLIN5 knockdown PDM across replicate fractions [threshold for clustered proteins was determined by significance between groups]. Right: Proteins were further grouped using k-means statistics breaking the PDM and PLIN5 knockdown PDM significant genes into 10 protein clusters. The clustered proteins were mapped to specific metabolic pathways using Panther Classification Overrepresentation testing.
(G) Mitochondrial fractions were analyzed by SDS-PAGE and immunoblotting for OXPHOS proteins and CPT-1α. n=3.
(H) Quantification of immunoblots of CM and PDM from control and PLIN5 knockdown samples. n=6-12. ns = $p>0.05$, *$p<0.05$, **$p<0.01$, ***$p<0.001$, ****$p<0.0001$.

Supplemental Figure 3

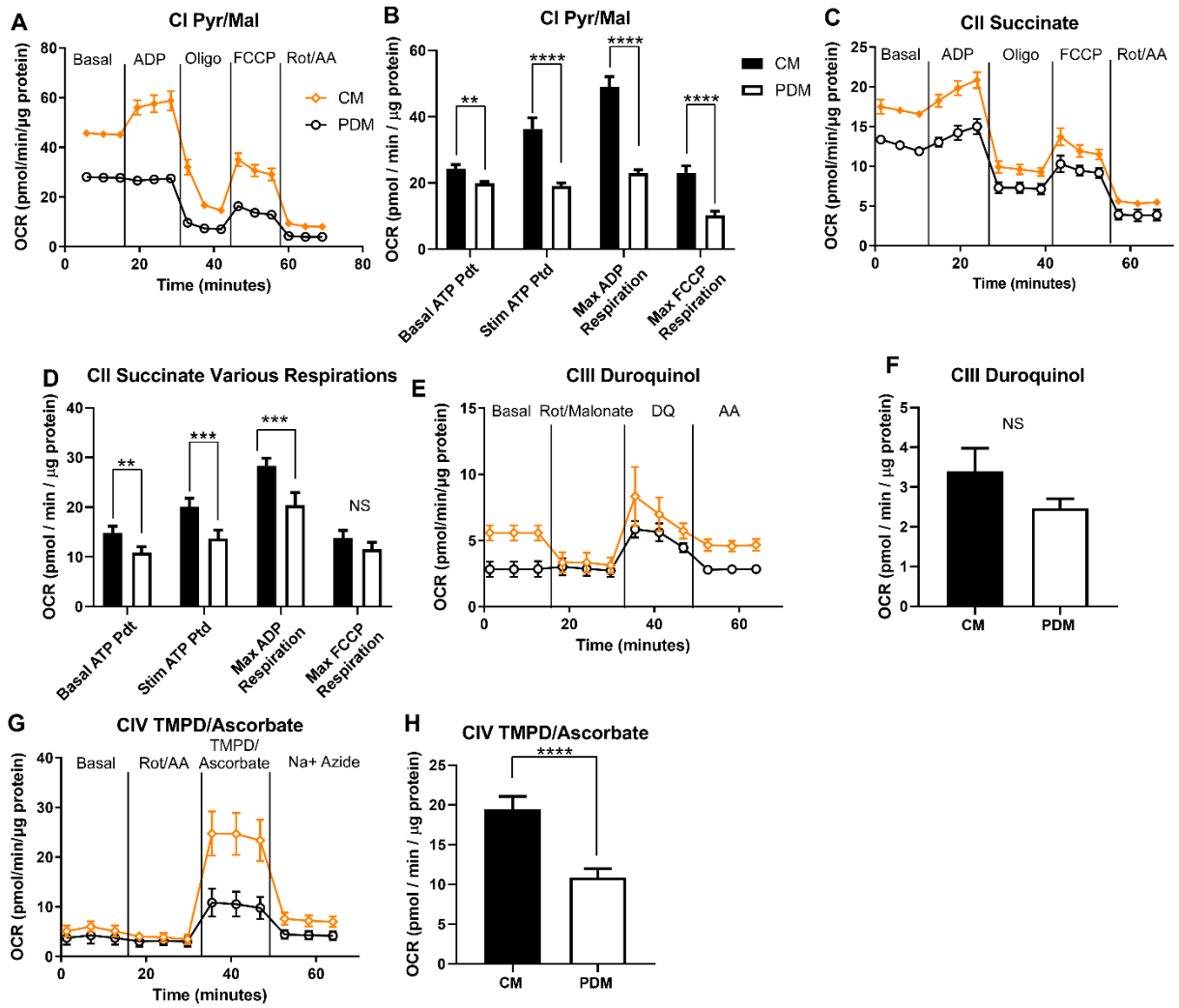

Figure S3. Cytosolic mitochondria have increased Supercomplex I, II, and IV activity (Related to Figure 1-2 and 7).

(A) Representative traces of oxygen consumption rates (OCRs) of isolated PDM and CM driven with pyruvate + malate. ADP, oligomycin, FCCP, and rotenone/antimycin were sequentially injected to assess mitochondrial respiratory states. n=6 technical replicates per group and repeated on three individual isolations.

(B) Quantification of average OCR at different mitochondrial respiratory states when pyruvate + malate was the fuel source in representative experiments.

(C) Representative traces of OCR of isolated PDM and CM were driven with succinate. ADP, oligomycin, FCCP, and rotenone/antimycin were sequentially injected to assess mitochondrial respiratory states. N=6 technical replicates per group and repeated on three individual isolations.

(D) Quantification of average OCR at different mitochondrial respiratory states when succinate was the fuel source in representative experiments.

€ Representative traces of oxygen consumption rates (OCRs) of isolated PDM and CM were driven with duroquinol. Rotenone/malonate, duroquinol, and antimycin were sequentially injected to

assess mitochondrial respiratory states (n=6 technical replicates per group and repeated on three individual isolations).
(F) Quantification of OCR at different mitochondrial respiratory states when duroquinol was the fuel source in representative experiments.
(G) Representative traces of oxygen consumption rates (OCRs) of isolated PDM and CM driven with TMPD + ascorbate. Rotenone/antimycin, TMPD/ascorbate, and sodium azide were sequentially injected to assess mitochondrial respiratory states. n=6 technical replicates per group and repeated on three individual isolations.
(H) Quantification of OCR at different mitochondrial respiratory states when TMPD + ascorbate was the fuel source in representative experiments.
ns = $p>0.05$, *$p<0.05$, **$p<0.01$, ***$p<0.001$, ****$p<0.0001$.

Supplemental Figure 4

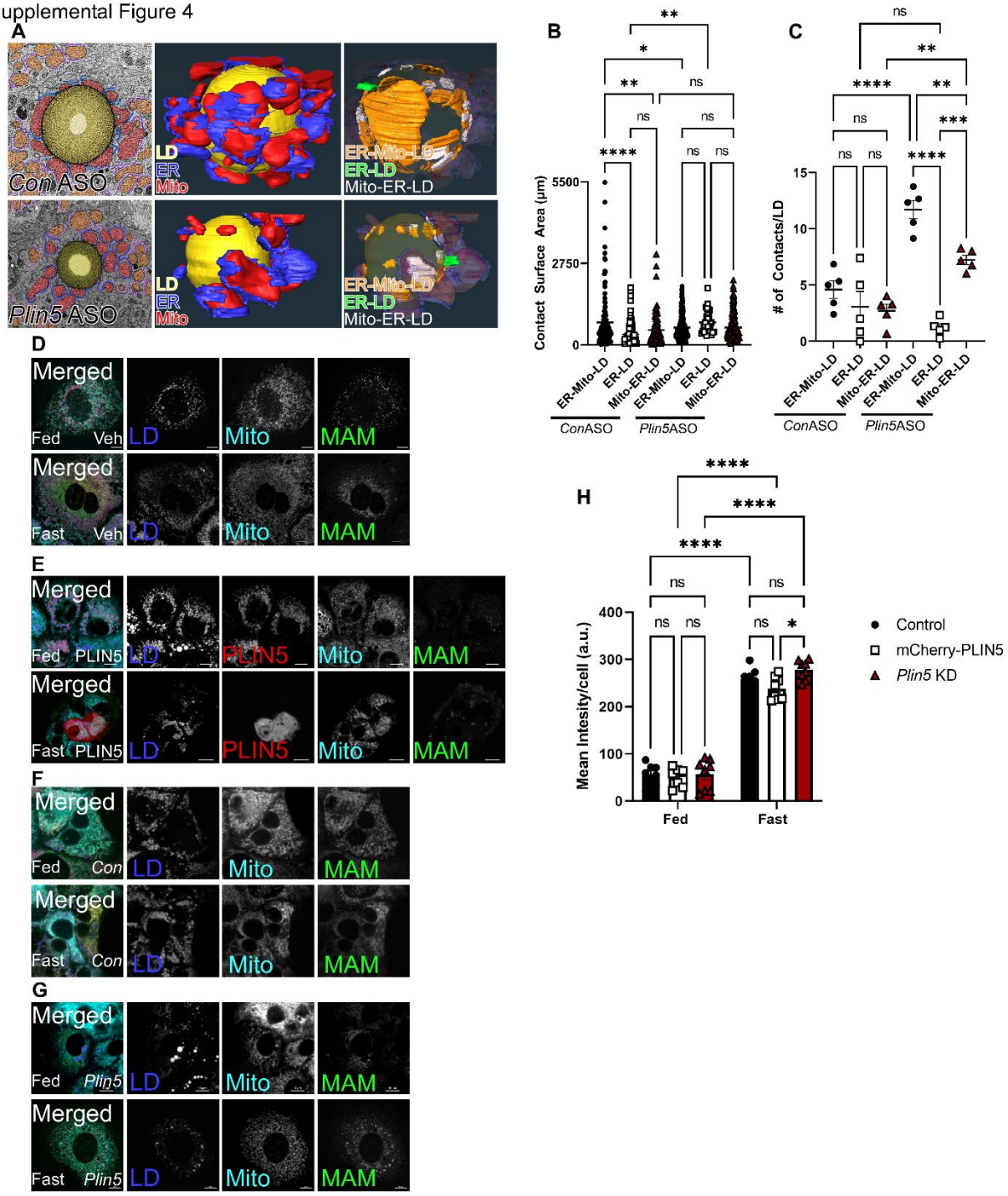

Figure S4. PLIN5 alters mitochondria-LD interactions but does not impact MAM formation (Related to Figure 5).

(A) Micrographs of LDs surrounded by PDM and CM from Control and PLIN5 ASO-treated mice fasted overnight; note that these experiments were down in parallel with those in Figure 5 and thus the same control is shown. Also shown are the 3D reconstructions of serial tomograms compiled as a single image. Blue=ER, red=mitochondria, yellow=LD. ER-Mito-LD (orange), ER-LD

(green), and mito-ER-LD (White) interactions were identified and segmented to render interaction maps in 3D and show in the far-right image.
(B) Quantitative analysis of the ER-mito-LD, ER-LD, and mito-ER-LD contacts. Quantification was determined from n=2 samples and 4 regions of interest examining the effect of PLIN5 knockdown.
(C) Quantitative analysis of the ER-mito-LD, ER-LD, and mito-ER-LD contacts per LD in each region of interest examining the effect of PLIN5 knockdown.
(D-E) Representative confocal microscopy images of mitochondria, LDs, and the MAM sensor (SPLICSs) in AML12 cells transfected with our null or mCherry-PLIN5 construct in fed and fasting media.
(F-G) Representative confocal microscopy images of mitochondria, LDs, and the MAM sensor in AML12 cells transfected with *control* or *Plin5* ASOs in fed and fasting media.
(H) Quantification of SPLICSs by total mean intensity per cell. n=6-8 images with 12-16 cells per condition.

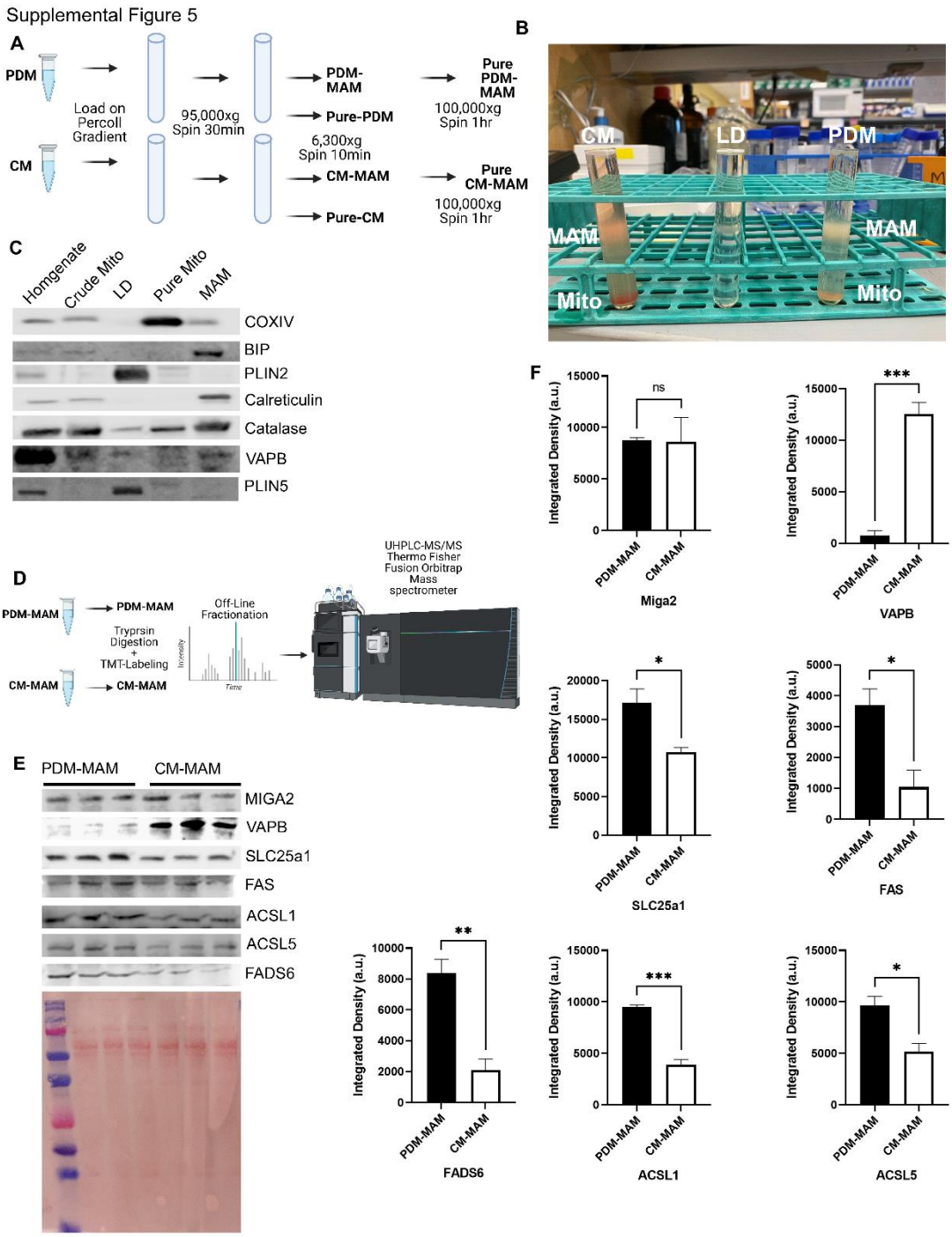

Figure S5. Cytosolic and peripdroplet mitochondria have unique MAMs (Related to Figure 7).

(A) Schematic of MAM isolation from CM and PDM.

(B) Picture of ultra-centrifugation tubes post 95,000xg spin. The MAM fraction is in the middle of the tube. Pure mitochondria pelleted at the bottom of the tube.

(C) Immunoblotting of cellular fractions to determine the purity of CM-MAM and PDM-MAM. Fractions were probed for Catalase (peroxisome), COXIV (mitochondria), BiP (MAM), PLIN2 (LD), PLIN5 (LD), Calreticulin (ER/MAM), and VAP-B (MAM).

(D) Schematic showing the further purification steps taken prior to LC-MS/MS, protein digestion, isobaric labeling of peptides, offline fractionation, and LC-MS/MS.
(E) Immunoblotting of PDM-MAM and CM-MAM for proteins identified in the proteomics experiment. Fractions were probed for MIGA2, VAP-B, SLC25a1, FAS, ACSL1, ACSL2, ACSL5, SCD1, FADS6, and AGPAT2. n=3.
(F) Quantification of immunoblots in part E. ns = $p>0.05$, *$p<0.05$, **$p<0.01$, ***$p<0.001$, ****$p<0.0001$.

Supplemental Figure 6

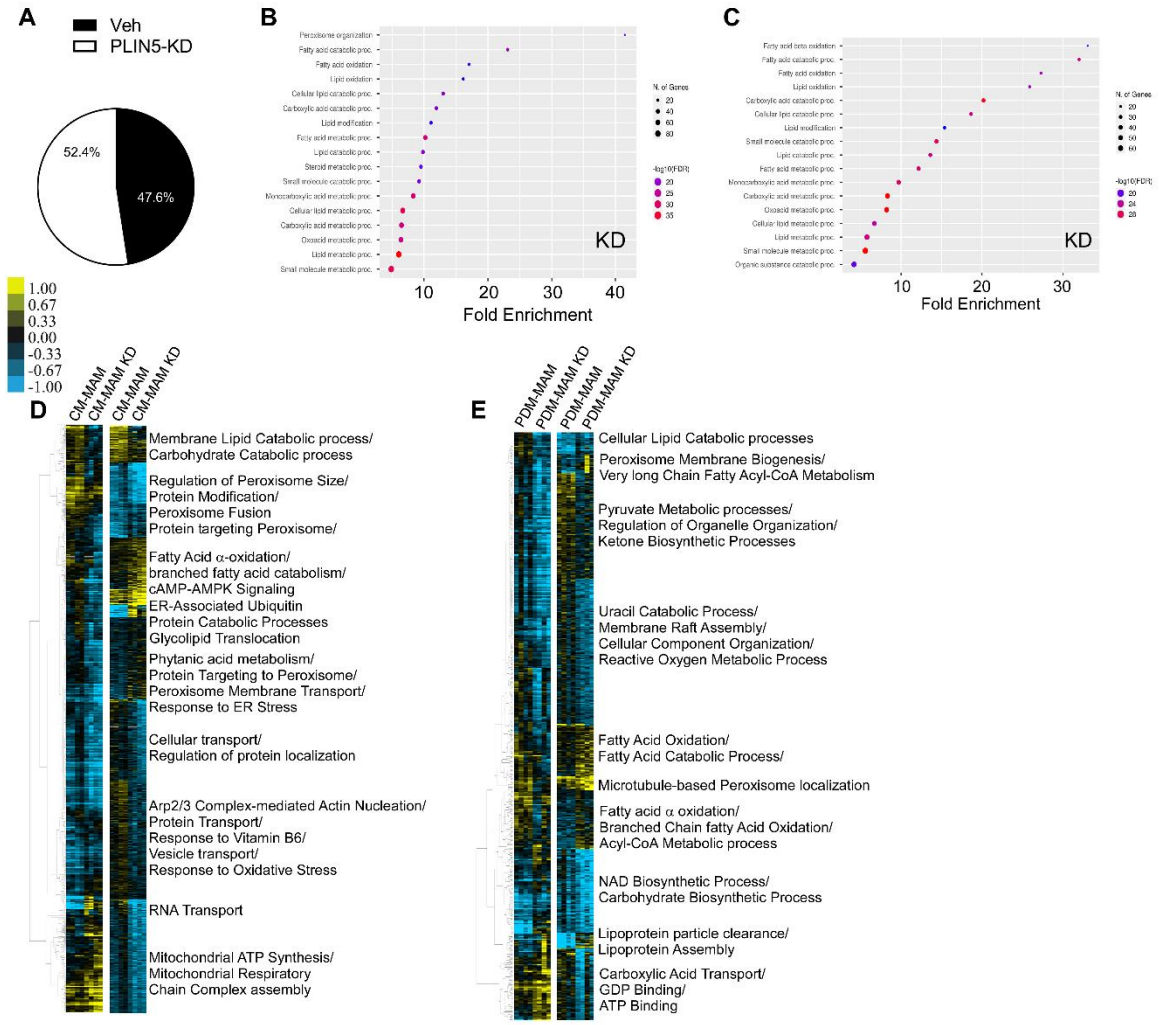

Figure S6. PLIN5 knockdown alters the proteomes of peridroplet and cytosolic MAMs (Related to Figure 7).

(A) Quantitative proteomics was performed on CM-MAM and PDM-MAM fractions isolated from control and PLIN5 ASO-treated mice. The effect of PLIN5 knockdown on CM-MAM and PDM-MAM proteomes as part of the entire data set is depicted in a pie chart. n=4 mitochondrial fractions isolated from independent mice.

(B) GO term pathway analysis of all significant proteins detected in the CM-MAM fraction (control CM-MAM vs PLIN5 knockdown CM-MAM).

(C) GO term pathway analysis of all significant proteins detected in the PDM-MAM fraction (control PDM-MAM vs PLIN5 knockdown PDM-MAM).

(D) Left: Hierarchical clustering of proteins significantly different between CM-MAM and PLIN5 knockdown CM-MAM across replicate fractions [threshold for clustered proteins was determined by significance between groups]. Right: Proteins were further grouped using k-means statistics breaking the CM-MAM and PLIN5 knockdown CM-MAM significant genes into 10 protein clusters. The clustered proteins were mapped to specific metabolic pathways using Panther Classification Overrepresentation testing.

(E) Left: Hierarchical clustering of proteins significantly different between PDM-MAM and PLIN5 knockdown PDM-MAM across replicate fractions [threshold for clustered proteins was determined by significance between groups]. Right: Proteins were further grouped using k-means statistics breaking the PDM-MAM and PLIN5 knockdown PDM-MAM significant genes into 10 protein clusters. The clustered proteins were mapped to specific metabolic pathways using Panther Classification Overrepresentation testing.

Supplemental Figure 7

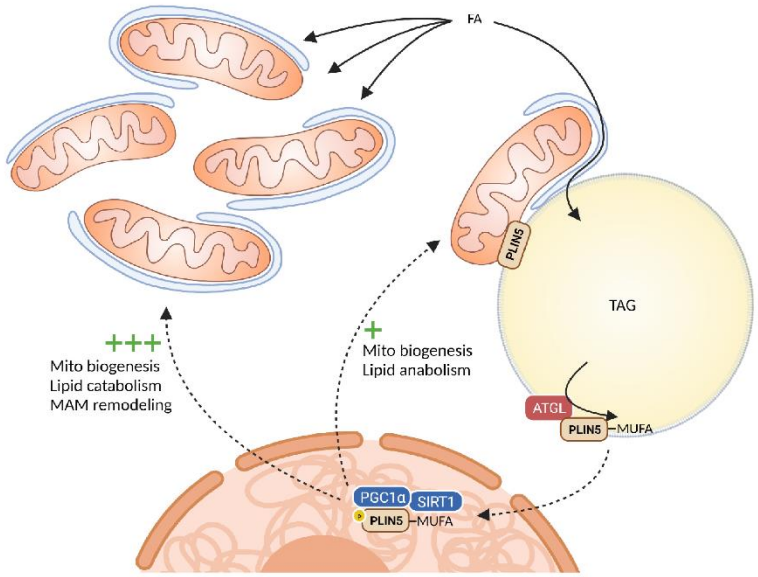

Figure S7. PLIN5 regulates mitochondrial pools (Related to Figure 2, 4, S2, S5, and S6). Schematic representation of the complex actions of PLIN5 in determining CM and PDM function. PLIN5 has been shown to regulate mitochondrial biogenesis through MUFA trafficking to the nucleus.[1] The current study supports the regulator role of PLIN5 as the CM and PDM proteomics data shows a normalization between the two mitochondrial populations - including the disruption in mitochondrial oxidative capacity as well as mitochondrial biogenesis - when PLIN5 is suppressed (See Figure 2 and S2). In line with the signaling properties of PLIN5, knockdown of PLIN5 dramatically altered MAM associated with both the PDM and CM disrupting β-oxidation, mitochondrial protein import, as well as translation processes. Regarding lipid incorporation, PLIN5 knockdown blunted FA esterification into complex lipid species (Figure 4). The mechanism by which PLIN5 knockdown blunted FA storage was through destabilization of mitochondria-LD interactions. Total numbers of mitochondria-LD interactions increased but the total surface area between the organelles was reduced. In support of our findings, work from[2] and [3] expressing a LD-mitochondrial non-tethering variant of PLIN5 or completely ablating the protein show decreased mitochondrial interactions and decreased lipid storage capacity. Together, data from the current study supports the role of PLIN5 in nuclear signaling to govern mitochondrial biogenesis as well as mitochondria-LD tethering to facilitate efficient lipid storage.

1. Najt, C.P., Khan, S.A., Heden, T.D., Witthuhn, B.A., Perez, M., Heier, J.L., Mead, L.E., Franklin, M.P., Karanja, K.K., Graham, M.J., et al. (2019). Lipid Droplet-Derived Monounsaturated Fatty Acids Traffic via PLIN5 to Allosterically Activate SIRT1. Molecular Cell. https://doi.org/10.1016/j.molcel.2019.12.003.
2. Benador, I.Y., Veliova, M., Mahdaviani, K., Petcherski, A., Wikstrom, J.D., Assali, E.A., Acín-Pérez, R., Shum, M., Oliveira, M.F., Cinti, S., et al. (2018). Mitochondria Bound to Lipid Droplets Have Unique Bioenergetics, Composition, and Dynamics that Support Lipid Droplet Expansion. Cell Metabolism *27*, 869-885.e866. https://doi.org/10.1016/j.cmet.2018.03.003.
3. Keenan, S.N., Meex, R.C., Lo, J.C.Y., Ryan, A., Nie, S., Montgomery, M.K., and Watt, M.J. (2019). Perilipin 5 Deletion in Hepatocytes Remodels Lipid Metabolism and Causes Hepatic Insulin Resistance in Mice. Diabetes *68*, 543-555. 10.2337/db18-0670.